Phys Chem Minerals (2015) 42:327–336
DOI 10.1007/s00269-014-0723-8

ORIGINAL PAPER

Equation of state of $Ca_2AlSiO_{5.5}$ oxygen defect perovskite

Chaowen Xu · Shuangmeng Zhai · Lijin Ye · Yuji Higo

Received: 10 June 2014 / Accepted: 10 November 2014 / Published online: 19 November 2014

Abstract The elastic properties of synthetic low-pressure and high-pressure $Ca_2AlSiO_{5.5}$ oxygen defect perovskites were investigated by in situ X-ray diffraction in a large-volume high-pressure apparatus. The *P–V–T* data were collected up to 22.75 GPa at room temperature, up to 12.88 GPa and 1,300 K for low-pressure phase and up to 25.76 GPa at room temperature for high-pressure phase. The *P–V* data at room temperature were fitted using a third-order Birch–Murnaghan equation of state to obtain $K_0 = 146.1(9)$ GPa and $K_0' = 3.64(9)$ for the monoclinic low-pressure phase, and $K_0 = 150.4(19)$ GPa and $K_0' = 3.16(23)$ for the rhombohedral high-pressure phase. If K_0' was fixed at 4.0, the isothermal bulk moduli were obtained as 142.6(3) and 144.0(8) GPa for low-pressure and high-pressure phase, respectively. Both the low-pressure and high-pressure $Ca_2AlSiO_{5.5}$ oxygen defect perovskites are much softer than pure $CaSiO_3$ perovskite. The *P–V–T* data of low-pressure phase were fitted by the high-temperature Birch–Murnaghan equation of state to get thermoelastic properties as $V_0 = 827.0(3)$ Å^3, $K_T = 146.8(22)$ GPa, $K_T' = 3.55(21)$, $(\partial K_T/\partial T)_P = -0.037(2)$ GPa/K and $\alpha_T = 7.67(20) \times 10^{-5} - 3.20(30) \times 10^{-8}\,T$. Based on the results, the density profiles of low-pressure and high-pressure $Ca_2AlSiO_{5.5}$ oxygen defect perovskites were calculated and compared with those of some mantle silicate minerals to discuss the potential occurrence of $Ca_2AlSiO_{5.5}$ oxygen defect perovskite in the Earth's interior.

Keywords $Ca_2AlSiO_{5.5}$ · Oxygen defect perovskite · In situ X-ray diffraction · Equation of state

C. Xu · L. Ye
Key Laboratory of Orogenic Belts and Crustal Evolution, MOE; School of Earth and Space Sciences, Peking University, Beijing 100871, China

S. Zhai (✉)
Key Laboratory of High-Temperature and High-Pressure Study of the Earth's Interior, Institute of Geochemistry, Chinese Academy of Sciences, Guiyang 550002, Guizhou, China
e-mail: zhaishuangmeng@vip.gyig.ac.cn

Y. Higo
Japan Synchrotron Radiation Research Institute, Sayo, Hyogo 679-5198, Japan

Introduction

It is well known that Ca-perovskite is an important constituent mineral in the deep Earth's mantle. Under the lower mantle conditions, Ca-perovskite is 5–7 wt% in the peridotitic mantle and 22–29 wt% in the subducted mid-oceanic ridge basalt (MORB) (Hirose 2002; Hirose and Fei 2002). Moreover, Ca-perovskite-dominated material may exist at the core–mantle boundary (Noguchi et al. 2013). The physical and chemical properties of Ca-perovskite have been widely studied (Mao et al. 1989; Kesson et al. 1995; Akber-Knutson et al. 2002; Stixrude et al. 2007; Kudo et al. 2012).

It is noted that in $CaSiO_3$ perovskite, the Si^{4+} cation can be substituted by trivalent cations, such as Al^{3+} and Fe^{3+}, i.e., $2Si^{4+} = 2M^{3+} + V_O$, where V_O represents oxygen vacancy balancing the charge (Bläß et al. 2007). Actually, Fitz Gerald and Ringwood (1991) synthesized a high-pressure $Ca_2AlSiO_{5.5}$ oxygen defect perovskite at 1,973 K and 16 GPa, in which 50 % silicon was exchanged by aluminum. This phase had a parental cubic structure, but a rhombohedral defect perovskite with a fivefold superstructure developed along the pseudo-cubic {111} direction, and the Si and Al distributed randomly in octahedral sites (Fitz Gerald and Ringwood 1991). The low-pressure $Ca_2AlSiO_{5.5}$ oxygen defect perovskite was obtained and depicted as an

intermediate structure between $Ca_2Si_2O_6$ cubic perovskite and $Ca_2Al_2O_5$ brownmillerite-type phase (Bläß et al. 2004, 2007). Based on synchrotron power X-ray diffraction data using information from NMR as constraints, Kanzaki et al. (2012) refined the monoclinic low-pressure $Ca_2AlSiO_{5.5}$ oxygen defect perovskite (space group of *C2/c*) as double layers of octahedra and double layers of tetrahedra, stacked alternatively in the [111] direction of cubic perovskite to form eightfold superstructure, where each tetrahedron has one non-bridging-oxygen. The Si atoms locate in tetrahedral site, and Al atoms locate in octahedra sites. Kojitani et al. (2009) determined the phase boundary between the low-pressure and high-pressure $Ca_2AlSiO_{5.5}$ oxygen defect perovskites, and their result showed that the high-pressure phase was stable at least in the transition zone since no further higher pressure and temperature results are available.

The concentration and aggregation of oxygen defects might significantly affect physical and chemical properties of perovskite-structured materials (Navrotsky 1999; Brodholt 2000). However, little information about the physical properties of oxygen defect Ca-bearing perovskite under high-pressure condition is available. In this paper, the pressure–volume–temperature relationships of low-pressure $Ca_2AlSiO_{5.5}$ oxygen defect perovskite and pressure–volume relation of high-pressure $Ca_2AlSiO_{5.5}$ oxygen defect perovskite were investigated by in situ energy-dispersive X-ray diffraction measurements in multianvil high-pressure apparatus combined with synchrotron radiation at the BL04B1 beamline of SPring-8, Japan. The experiments were conducted up to 22.75 GPa at room temperature, up to 12.88 GPa and 1,300 K for low-pressure phase and up to 25.76 GPa at room temperature for high-pressure phase. The obtained *P–V–T* data were analyzed by using Birch–Murnaghan equation of state (EoS). The results were compared with those of $CaSiO_3$ perovskite. Meanwhile, the density profiles of $Ca_2AlSiO_{5.5}$ oxygen defect perovskites were calculated based on the obtained results and compared with those of some mantle silicate minerals to discuss the potential occurrence of $Ca_2AlSiO_{5.5}$ oxygen defect perovskite in the Earth's interior.

Experimental

The low-pressure and high-pressure $Ca_2AlSiO_{5.5}$ oxygen defect perovskites were synthesized at 10 GPa and 1,573 K, and 15 GPa and 1,673 K, respectively, as described by Kojitani et al. (2009). A mixture of each sample plus 10 wt% Au, which was used as pressure marker, was prepared as staring material for in situ X-ray experiments.

The high-pressure energy-dispersive X-ray diffraction experiments were carried out using a multianvil apparatus, SPEED-1500, installed at the BL04B1 beamline of SPring-8. Eight tungsten carbide cubes with edge length of 26 mm and truncated edge length of 4 or 3 mm were used as second-stage anvils. The high-pressure system is combined with a synchrotron radiation source and an energy-dispersive X-ray diffraction system with a Ge solid-state detector (SSD) and a charge coupled devise (CCD) camera for radiographic imaging of the sample. A polychromatic X-ray beam collimated to the dimensions of 0.05 mm horizontally and 0.2 mm vertically was directed to the sample through pyrophyllite gasket and pressure medium. A multichannel analyzer was used to acquire photons in a range of 30–150 keV, which was calibrated with characteristic fluorescence X-ray lines of several reference metals, including Cu, Mo, Ag, Ta, Pt, Au and Pb. The precision of the energy measurements was approximately ±30 eV per channel. The 2θ angle of SSD was set at ~6° with respect to the incident beam direction and accurately calibrated using known diffraction peaks from a standard material such as gold. The uncertainty of the diffraction angle after calibration was typically ±0.002°.

The 10- or 7-mm edge length semi-sintered octahedron made of MgO + 5 wt% Cr_2O_3 was used as the pressure medium, and pyrophyllite was used as the gasket. TiB_2 + BN + AlN (BN composite heater EC, Denki Kagaku Kogyo Co) was adopted as a tubing heater and sample capsule due to its transparency for X-ray. The initial size of cylindrical sample is 1.0 mm in diameter and 1.5 mm in length. The in situ experimental procedure was similar to previous studies by Zhai et al. (2011, 2013). The W_3Re_{97}–$W_{25}Re_{75}$ thermocouple was used to monitor the temperature and its junction centered in the mixture of the sample and the pressure calibrant. For *P–V* relationship, the sample assembly was heated to 1,000 K for releasing deviatoric stress accumulated during the compression steps. The sample was quenched to room temperature after keeping at 1,000 K for about 10 min. For *P–V–T* relationship, the sample was first squeezed at room temperature and then heated to 1,300 K. Following this, the temperature was first decreased to 1,100 K and then to 300 K in step of 200 K. The press load was increased after the first data collection cycle, and then, the temperature was increased to 1,300 K to start another data collection cycle during cooling. A few data collection cycles were carried out in the same way. The measured *P–T* paths are shown in Fig. 1. At each *P–T* condition, an X-ray diffraction pattern was collected. The in situ X-ray profiles were processed by SSD Profile Analysis and X-ray Analysis Program. The lattice parameters were obtained by Unitcell program (Holland and Redfern 1997). Pressure was calculated from the EoS of gold proposed by Tsuchiya (2003) and the volume determined by using (1 1 1), (2 0 0), (2 2 0), (3 1 1), (2 2 2), (3 3 1) and (4 2 0) diffraction lines of gold. In some cases, one or two lines were unavailable to determine pressure when

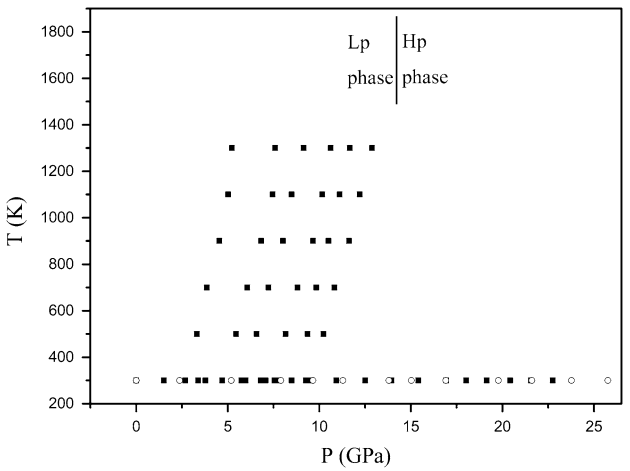

Fig. 1 *P–T* paths of the in situ X-ray diffraction experiment. *Solid squares* and *open circles* represent the data points of low-pressure and high-pressure $Ca_2AlSiO_{5.5}$ oxygen defect perovskite, respectively. *Solid line* represents the phase boundary between low-pressure and high-pressure $Ca_2AlSiO_{5.5}$ oxygen defect perovskite determined by Kojitani et al. (2009)

the diffraction peaks of gold overlapped with those of the sample. Uncertainties in the pressure determination were mostly within ±0.10 GPa. It should be noted that the thermocouple in the experiment of high-pressure $Ca_2AlSiO_{5.5}$ oxygen defect perovskite cuts during compression and then the annealing temperature was estimated from the temperature–power relation of heater.

Results and discussion

Totally 55 X-ray diffraction patterns of low-pressure $Ca_2AlSiO_{5.5}$ oxygen defect perovskite were collected under various pressure–temperature conditions, and 13 X-ray diffraction patterns of high-pressure $Ca_2AlSiO_{5.5}$ oxygen defect perovskite were collected under various pressures and room temperature in this study. The typical X-ray diffraction patterns are illustrated in Fig. 2. The X-ray diffraction pattern at ambient conditions was obtained after the sample was completely decompressed and taken out of the cell assembly. The main diffraction peaks of the sample are sharp and clear for precisely determining the lattice parameters. For low-pressure phase, the sample peaks of (3 1 −1), (3 1 1), (2 2 0), (1 1 7), (4 0 4), (2 2 −8), (1 3 5), (2 4 6) and (6 2 −2) were used for lattice parameter calculation, and for high-pressure phase, the sample peaks of (3 3 4), (1 1 3), (2 4 4), (1 1 −2) and (6 6 8) were adopted. Other peaks of sample were not adopted due to the overlap, as shown in Fig. 2. In order to confirm whether the sample was stable at 1,000 K and pressures higher than 14 GPa where the low-pressure monoclinic phase may transform to high-pressure rhombohedral phase, the diffraction patterns were carefully checked and no new peaks appeared or peaks disappeared. It implies that low-pressure monoclinic phase was stable in the present P–T conditions probably due to the kinetics since the temperature of 1,000 K is not high enough. The powder X-ray diffraction patterns at ambient conditions revealed that the low-pressure $Ca_2AlSiO_{5.5}$ phase has a monoclinic structure with unit-cell dimensions of $a = 9.129(1)$ Å, $b = 5.2313(3)$ Å, $c = 17.609(1)$ Å, $\beta = 100.472(8)°$ and $V = 826.99(13)$ Å^3 and the high-pressure phase has a rhombohedral structure with $a = 11.1757(3)$, $\alpha = 27.152(4)°$ and $V = 1{,}105.16(11)$ Å^3. These unit-cell parameters are consistent with the results reported by Bläß et al. (2007) [i.e., $a = 9.1357(2)$ Å, $b = 5.2225(1)$ Å, $c = 17.505(1)$ Å, $\beta = 100.02(1)°$ for monoclinic phase] and Fitz Gerald and Ringwood (1991) (i.e., $a = 11.12$ Å and $\alpha = 27.27°$ for rhombohedral phase).

P–V data at room temperature

The high-pressure data of low-pressure and high-pressure $Ca_2AlSiO_{5.5}$ oxygen defect perovskites were collected up to 22.75 and 25.76 GPa at ambient temperature after annealing, respectively. The effect of pressure on the unit-cell parameters and volume is shown in Tables 1 and 2, respectively. It is noted that the effect of pressure on the variation of α and β angle is quite small. During compression, the value of α and β angle is nearly constant. The *P–V* data at room temperature was fitted to a third-order Birch–Murnaghan EoS (Birch 1947) in the following form:

$$P(V) = \frac{3K_0}{2}\left[\left(\frac{V_0}{V}\right)^{\frac{7}{3}} - \left(\frac{V_0}{V}\right)^{\frac{5}{3}}\right]\left\{1 + \frac{3}{4}(K_0' - 4)\left[\left(\frac{V_0}{V}\right)^{\frac{2}{3}} - 1\right]\right\} \quad (1)$$

where K_0, K_0' and V_0 are the isothermal bulk modulus, its pressure derivation and the unit-cell volume at ambient conditions, respectively. A least-squares fitting using an EosFit program (Angel 2001) gives $V_0 = 826.9(1)$ Å^3, $K_0 = 146.1(9)$ GPa and $K_0' = 3.64(9)$ for low-pressure phase, and $V_0 = 1{,}105.2(2)$ Å^3, $K_0 = 150.4(19)$ GPa and $K_0' = 3.16(23)$ for high-pressure phase. The unit-cell volume data as a function of pressure and the compression curves for both samples are plotted in Fig. 3. If the K_0' was set as 4, the isothermal bulk moduli were obtained as 142.6(3) and 144.0(8) GPa for low-pressure and high-pressure phase. The isothermal bulk modulus of high-pressure phase is higher than that of the low-pressure phase in this study, which is reasonable since the structure becomes tighter due to the phase transition from monoclinic low-pressure phase to rhombohedral high-pressure phase.

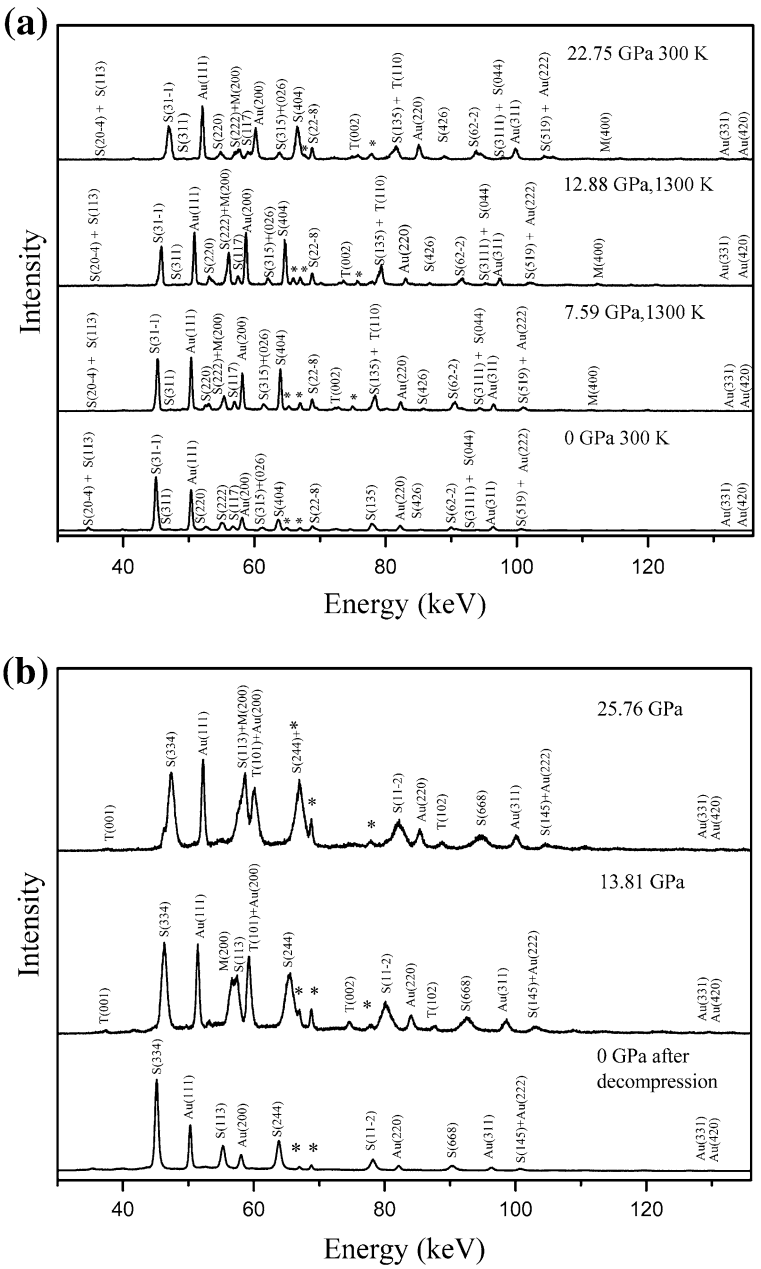

Fig. 2 Typical X-ray diffraction patterns of low-pressure (**a**) and high-pressure (**b**) $Ca_2AlSiO_{5.5}$ oxygen defect perovskite in this study. Abbreviations indexed to the diffraction peaks: *S* $Ca_2AlSiO_{5.5}$, *Au* gold, *asterisk* X-ray fluorescence of gold, *M* MgO, *T* TiB_2

In order to evaluate the quality of the Birch–Murnaghan EoS fitting, the relationships between the Eulerian strain (f_E) and the normalized pressure ($F = P/[3f_E\,(2f_E + 1)^{5/2}]$) for both phases are plotted in Fig. 4. The f_E–F plot provides a visual indication to whether higher order terms, such as K_0' and K_0'' (the isothermal bulk modulus' second-order pressure derivation at ambient conditions), are significant in the EoS. The small negative slope of the f_E–F plot indicates that the first pressure derivative of the bulk modulus is lower than 4. Therefore, the values of the derived K_0', 3.64(9) for low-pressure phase and 3.16(23) for high-pressure phase, are consistent with the f_E–F plot analysis. The slope of low-pressure phase is shallower than that of high-pressure phase, implying the derived K_0' of low-pressure phase is larger than that of high-pressure phase. It is consistent with the fitted results.

The bulk moduli of low-pressure and high-pressure $Ca_2AlSiO_{5.5}$ oxygen defect perovskites are much lower than that of $CaSiO_3$ perovskite, as shown in Table 3. Compared with that of $CaSiO_3$ perovskite, the isothermal bulk moduli of low-pressure and high-pressure $Ca_2AlSiO_{5.5}$ decrease about 90 GPa. Due to the substitution of Si^{4+} by Al^{3+}, oxygen vacancies generate in $Ca_2AlSiO_{5.5}$, which largely affects the isothermal bulk modulus, as observed in the Mg-bearing silicate perovskites (Zhang and Weidner 1999; Andrault et al. 2007). Similarly, such large decrease

Table 1 Pressure, temperature, lattice parameters and unit-cell volume of low-pressure $Ca_2AlSiO_{5.5}$ oxygen defect perovskite

P (GPa)	T (K)	a (Å)	b (Å)	c (Å)	β (°)	V (Å^3)
0.00	300	9.129(1)	5.2313(3)	17.609(1)	100.472(8)	826.99(13)
1.51(8)	300	9.117(2)	5.2187(9)	17.478(2)	100.173(9)	818.53(13)
3.38(7)	300	9.075(2)	5.1952(9)	17.443(2)	100.551(8)	808.43(11)
3.78(6)	300	9.063(2)	5.1939(9)	17.421(2)	100.279(9)	806.88(13)
5.23(3)	1,300	9.199(2)	5.2423(3)	17.554(2)	100.442(8)	832.49(12)
5.02(3)	1,100	9.198(1)	5.2335(3)	17.579(2)	100.724(8)	831.43(12)
4.54(7)	900	9.176(1)	5.2271(3)	17.529(2)	100.709(8)	826.10(12)
3.86(7)	700	9.145(1)	5.2275(3)	17.543(2)	100.622(8)	824.32(12)
3.31(6)	500	9.116(1)	5.2127(3)	17.542(2)	100.646(8)	819.20(12)
2.68(6)	300	9.090(1)	5.2002(3)	17.467(2)	100.392(9)	812.13(12)
5.77(5)	300	9.029(1)	5.1617(9)	17.370(2)	100.172(9)	796.82(13)
6.80(7)	300	9.016(1)	5.1551(9)	17.310(2)	100.110(9)	792.05(13)
7.59(5)	1,300	9.126(1)	5.2127(3)	17.491(2)	100.605(8)	817.96(12)
7.45(5)	1,100	9.128(1)	5.1994(3)	17.502(2)	100.649(8)	816.18(12)
6.83(1)	900	9.098(1)	5.2011(3)	17.475(2)	100.638(8)	812.73(12)
6.07(4)	700	9.101(1)	5.1938(3)	17.496(2)	100.729(8)	812.50(12)
5.46(4)	500	9.072(1)	5.1913(3)	17.454(2)	100.609(8)	807.92(12)
4.70(8)	300	9.041(2)	5.1820(9)	17.403(2)	100.324(9)	802.14(13)
5.75(4)	300	9.030(2)	5.1638(9)	17.379(2)	100.330(9)	797.20(13)
7.84(7)	300	8.983(1)	5.1523(9)	17.279(2)	100.036(9)	787.47(13)
9.14(5)	1,300	9.109(1)	5.1945(3)	17.394(2)	100.380(8)	809.52(12)
8.49(7)	1,100	9.104(1)	5.1956(3)	17.426(2)	100.585(8)	810.22(12)
8.02(9)	900	9.073(1)	5.1890(3)	17.446(2)	100.586(8)	807.39(12)
7.23(4)	700	9.082(1)	5.1873(3)	17.425(2)	100.654(8)	806.72(12)
6.58(5)	500	9.061(2)	5.1687(3)	17.439(2)	100.700(8)	802.52(12)
5.98(4)	300	9.029(1)	5.1616(9)	17.369(2)	100.383(9)	796.12(13)
9.27(6)	300	8.955(1)	5.1447(9)	17.221(2)	100.296(9)	780.61(13)
10.62(2)	1,300	9.025(1)	5.1915(3)	17.371(2)	100.290(8)	800.81(12)
10.16(6)	1,100	9.045(1)	5.1783(3)	17.392(2)	100.591(8)	800.73(12)
9.66(7)	900	9.064(1)	5.1637(3)	17.366(2)	100.651(8)	798.79(12)
8.81(5)	700	9.052(1)	5.1754(3)	17.360(2)	100.651(8)	799.24(12)
8.16(7)	500	9.020(1)	5.1677(3)	17.341(2)	100.546(8)	794.62(11)
7.56(9)	300	8.988(1)	5.1539(9)	17.289(2)	100.146(9)	788.33(13)
11.67(6)	1,300	8.991(1)	5.1747(3)	17.359(2)	100.350(8)	794.50(11)
11.11(3)	1,100	9.027(1)	5.1622(3)	17.361(2)	100.523(8)	795.38(12)
10.50(5)	900	9.039(1)	5.1589(3)	17.333(2)	100.678(8)	794.25(12)
9.84(5)	700	9.039(1)	5.1550(3)	17.329(2)	100.709(8)	793.43(12)
9.36(7)	500	9.026(1)	5.1444(3)	17.303(2)	100.647(8)	789.64(11)
8.49(4)	300	8.972(1)	5.1503(9)	17.237(2)	100.003(9)	784.40(13)
12.88(4)	1,300	8.989(1)	5.1625(3)	17.298(2)	100.337(8)	789.66(11)
12.21(5)	1,100	8.987(1)	5.1618(3)	17.303(2)	100.464(8)	789.34(11)
11.63(4)	900	9.003(1)	5.1537(3)	17.302(2)	100.605(8)	789.06(11)
10.83(5)	700	9.013(1)	5.1561(3)	17.286(2)	100.524(8)	789.86(11)
10.23(5)	500	8.978(1)	5.1394(3)	17.322(2)	100.726(8)	785.31(11)
9.55(3)	300	8.952(1)	5.1408(9)	17.214(2)	100.190(9)	779.72(13)
10.93(4)	300	8.934(1)	5.1222(9)	17.174(2)	100.060(9)	773.78(12)
12.51(11)	300	8.917(1)	5.1132(9)	17.131(2)	100.655(9)	767.61(12)
13.95(9)	300	8.901(1)	5.0897(9)	17.081(2)	100.489(9)	760.92(12)
15.41(5)	300	8.870(1)	5.0831(9)	17.044(2)	100.329(9)	756.01(12)
16.93(3)	300	8.845(1)	5.0638(9)	17.026(2)	100.153(9)	750.67(12)

Table 1 continued

P (GPa)	T (K)	a (Å)	b (Å)	c (Å)	β (°)	V (Å^3)
18.02(4)	300	8.828(1)	5.0577(3)	17.015(2)	100.570(8)	746.80(11)
19.14(7)	300	8.804(1)	5.0463(3)	16.989(2)	100.514(8)	742.15(11)
20.43(1)	300	8.787(1)	5.0355(3)	16.963(2)	100.486(8)	738.05(10)
21.56(5)	300	8.769(1)	5.0312(3)	16.917(2)	100.611(8)	733.61(10)
22.75(3)	300	8.749(1)	5.0306(3)	16.876(2)	100.498(8)	730.35(10)

The values in parentheses are standard deviations and refer to the last digit

Table 2 Lattice parameters of rhombohedral high-pressure $Ca_2AlSiO_{5.5}$ oxygen defect perovskite at various pressures

P (GPa)	a (Å)	V (Å^3)	α (°)
0.00	11.1757(3)	1,105.16(11)	27.152(4)
2.37(9)	11.1122(2)	1,088.54(10)	27.041(3)
5.19(10)	11.0524(2)	1,069.34(10)	27.130(6)
7.90(10)	10.9918(2)	1,052.35(10)	27.104(3)
9.65(8)	10.9565(2)	1,041.88(10)	27.124(1)
11.29(10)	10.9264(2)	1,032.42(10)	27.172(9)
13.80(2)	10.8815(2)	1,019.93(10)	27.161(4)
15.03(3)	10.8481(2)	1,012.03(9)	27.081(2)
16.91(6)	10.8201(2)	1,003.48(9)	27.123(5)
19.78(8)	10.7676(2)	989.33(9)	27.099(8)
21.61(8)	10.7379(2)	980.70(9)	27.127(6)
23.77(16)	10.7029(2)	970.71(9)	27.151(7)
25.76(13)	10.6706(2)	963.30(9)	27.073(4)

Number in parentheses represents the error of lattice parameters

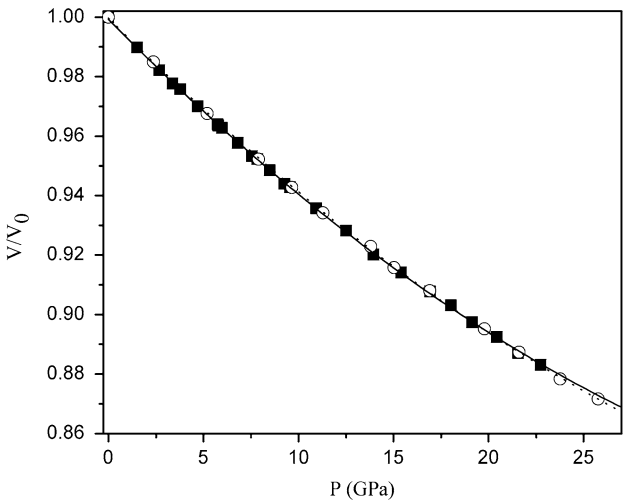

Fig. 3 *P–V* data of low-pressure (*solid squares*) and high-pressure (*open circles*) $Ca_2AlSiO_{5.5}$ oxygen defect perovskite at 300 K. *Solid curve* represents the third-order Birch–Murnaghan equation fit for low-pressure phase with $K_0 = 146.1(9)$ GPa and $K_0' = 3.64(9)$, and *dashed curve* represents the third-order Birch–Murnaghan equation fit for high-pressure phase with $K_0 = 150.4(19)$ GPa and $K_0' = 3.16(23)$. The uncertainties of pressure and volume are within *symbols*

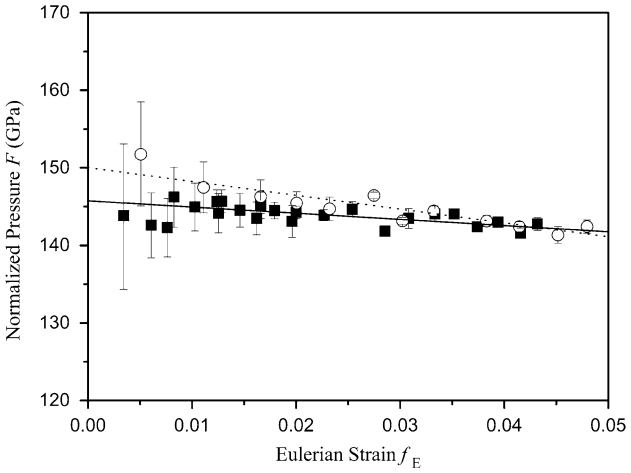

Fig. 4 Eulerian strain-normalized pressure (f_E–F) plot of $Ca_2AlSiO_{5.5}$ oxygen defect perovskite. *Solid squares* and *open circles* represent the data of low-pressure and high-pressure phase, respectively. *Solid* and *dashed lines* represent the linear fittings for low-pressure and high-pressure phase, respectively

in isothermal bulk modulus was reported for $Ca_2Fe_2O_5$ brownmillerite (Ross et al. 2002).

By fitting a "linearized" third-order Birch–Murnaghan EoS, simply by substituting the cube of the lattice parameter for the volume as in previous studies (Litasov et al. 2007; Zhai et al. 2011) and following the EosFit program (Angel 2001), axial compressibilities can be obtained. For the low-pressure $Ca_2AlSiO_{5.5}$ oxygen defect perovskite, the analysis yields that the c-axis ($K_c = 112 \pm 14$ GPa and $K' = 8.5 \pm 0.2$) is more compressible than the a-axis ($K_a = 152 \pm 7$ GPa and $K' = 2.5 \pm 0.6$) and b-axis ($K_b = 155 \pm 12$ GPa and $K' = 3.0 \pm 0.1$). As depicted by Kanzaki et al. (2012), oxygen is deficient at the middle of double SiO_4 layers, and each SiO_4 tetrahedral has one non-bridging oxygen in the c-direction. Therefore, the c-axis is more compressible than other two axes, which is consistent with the fitted results.

P–V–T relations of low-pressure $Ca_2AlSiO_{5.5}$ oxygen defect perovskite

Pressure–volume–temperature data were used to determine the thermoelastic properties of low-pressure $Ca_2AlSiO_{5.5}$

Table 3 Elastic parameters of $Ca_2AlSiO_{5.5}$ perovskite, compared with parameters of $CaSiO_3$ perovskite obtained from experimental studies

Composition	Structure	$K_{0,300}$ (GPa)	$K'_{0,300}$	References
$Ca_2AlSiO_{5.5}$	Monoclinic	146.1(9)	3.64(9)	This study
		142.6(3)	4.0(fixed)	This study
$Ca_2AlSiO_{5.5}$	Rhombohedral	150.4(19)	3.16(23)	This study
		144.0(8)	4.0(fixed)	This study
$CaSiO_3$	Cubic	232(8)	4.8(3)	Wang et al. (1996)
$CaSiO_3$	Cubic	236(4)	3.9(2)	Shim et al. (2000)
$CaSiO_3$	Tetragonal	255(5)	4(fixed)	Shim et al. (2002)
$CaSiO_3$	Cubic	207(4)	4.0(fixed)	Noguchi et al. (2013)

The parameters were fitted using Birch–Murnaghan EoS at 300 K except those from Noguchi et al. (2013) were fitted by Birch–Murnaghan EoS at 700 K

oxygen defect perovskite up to 12.88 GPa and 1,300 K. High-temperature Birch–Murnaghan (HTBM) EoS proposed by Saxena and Zhang (1990) was adopted with the following form:

$$P(V,T) = \frac{3K_T}{2}\left[\left(\frac{V_T}{V}\right)^{\frac{7}{3}} - \left(\frac{V_T}{V}\right)^{\frac{5}{3}}\right] \times \left\{1 + \frac{3}{4}\left(K'_T - 4\right)\left[\left(\frac{V_T}{V}\right)^{\frac{2}{3}} - 1\right]\right\} \quad (2)$$

where K_T, K'_T and V_T are the isothermal bulk modulus, its pressure derivative and the unit-cell volume at temperature T and ambient pressure, respectively, while V is the unit-cell volume at P and T. In Eq. (2), the bulk modulus pressure derivative K'_T is assumed to be constant against temperature, and therefore, $K'_T = K'_0$. The temperature effect on the bulk modulus is expressed by a linear function (Eq. 3), assuming that the temperature derivative is constant over the temperature range of the present study:

$$K_T = K_0 + \left(\frac{\partial K_T}{\partial T}\right)_P (T - 300) \quad (3)$$

The temperature derivative of the unit-cell volume V_T can be estimated by a function of the thermal expansion at ambient pressure α_T, which is empirically presented as: $\alpha_T = a_1 + a_2\,T$, where a_1 and a_2 are constant parameters, and

$$V_T = V_0 \exp \int_{300}^{T} \alpha_T \mathrm{d}T \quad (4)$$

A least-squares fitting of the data to the HTBM EoS yielded all six parameters [V_0, K_0, K'_0, $(\partial K_T/\partial T)_P$, a_1 and a_2] simultaneously. The thermoelastic parameters of low-pressure $Ca_2AlSiO_{5.5}$ oxygen defect perovskite are listed in Table 4, along with the values of the root-men-square (RMS) misfit in pressure. The results obtained from the HTBM EoS are consistent with those determined from fitting at room temperature. The obtained P–V–T data and the calculated isothermal compression curves at different temperatures are shown in Fig. 5. The observed data are reproduced well by the HTBM EoS. The thermoelastic parameters of pure $CaSiO_3$ perovskite are also listed in Table 4 for comparison.

It is interesting to note that the obtained thermal expansion is with a negative temperature dependence coefficient. It means that the thermal expansion coefficient decreases with increasing temperature. In low-pressure $Ca_2AlSiO_{5.5}$ oxygen defect perovskite monoclinic structure, vibration of Si and O atoms probably away from the linear Si–O–Si–O–Si axes is facilitated by O-vacancies and lead to obvious anisotropy. With temperature increasing, atomic thermal vibration intensifies and the distance between Si–Si becomes smaller.

Table 4 Thermoelastic parameters of low-pressure $Ca_2AlSiO_{5.5}$ oxygen defect perovskite compared with those of $CaSiO_3$ perovskite

	This study	Wang et al. (1996)	Shim et al. (2000)	Ricolleau et al. (2009)	Noguchi et al. (2013)
Composition	$Ca_2AlSiO_{5.5}$	$CaSiO_3$	$CaSiO_3$	$CaSiO_3$	$CaSiO_3$
Structure	Monoclinic	Cubic	Cubic	Tetragonal	Cubic
$V_{0,T}$ (Å^3)	827.0(3)	45.58(4)	27.45(2)	45.60(fixed)	46.5(1)
$K_{0,T}$ (GPa)	146.8(22)	232(8)	236(4)	244(1)	207(4)
$K'_{0,T}$	3.55(21)	4.8(3)	3.9(2)	4(fixed)	4(fixed)
$(\partial K_T/\partial T)_P$ (GPa K^{-1})	−0.037(2)	−0.036(8)	−0.028(11)	−0.035(2)	
a_1 (10^{-5} K^{-1})	7.67(20)	3.55(18)	2.2(3)	3.06(19)	5.7(5)
a_2 (10^{-8} K^{-2})	−3.20(30)			0.87(18)	
RMS misfit (GPa)	0.121				

The composition in the study of Ricolleau et al. (2009) was not pure $CaSiO_3$

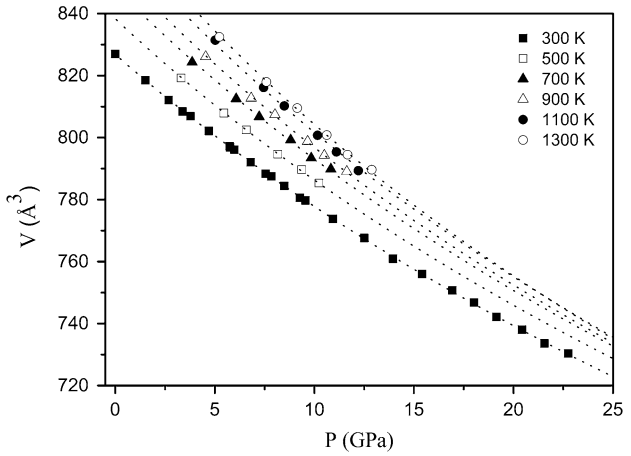

Fig. 5 *P–V–T* data fitted to HTBM EoS at various temperatures. The *error bars* are smaller than the size of the symbols. The *dashed lines* represent isothermal compression curves at 300, 500, 700, 900, 1,100 and 1,300 K, respectively, with the parameters listed in Table 4

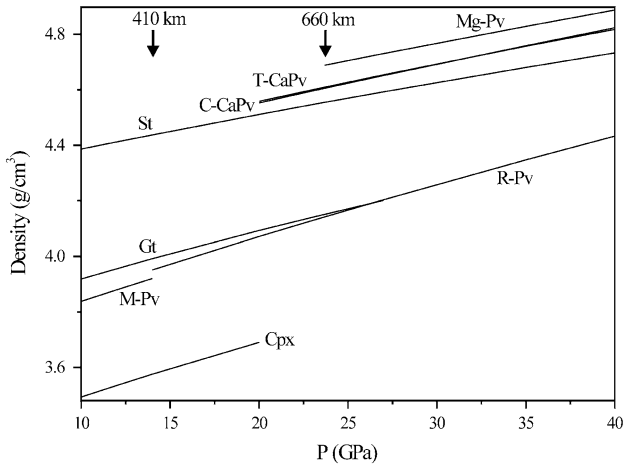

Fig. 6 Calculated density profiles of $Ca_2AlSiO_{5.5}$ oxygen defect perovskite and other silicate minerals as a function of pressure at room temperature. The phase abbreviations are as follows: *M-Pv* monoclinic low-pressure $Ca_2AlSiO_{5.5}$ oxygen defect perovskite, *R-Pv* rhombohedral high-pressure $Ca_2AlSiO_{5.5}$ oxygen defect perovskite, *Cpx* clinopyroxene, *Gt* majoritic garnet, *St* stishovite, *C-CaPv* cubic $CaSiO_3$ perovskite, *T-CaPv* tetragonal $CaSiO_3$ perovskite, *Mg-Pv* $MgSiO_3$ perovskite

Therefore, the unit-cell volume may shrink in certain direction and expand in other directions, and finally the whole structure shows a negative temperature dependence coefficient. Further studies are required to investigate the mechanism of the negative temperature dependence coefficient.

Density of $Ca_2AlSiO_{5.5}$ oxygen defect perovskite

Based on the elastic parameters obtained in the present study, the density profiles of both low-pressure and high-pressure $Ca_2AlSiO_{5.5}$ oxygen defect perovskites were calculated, as illustrated in Fig. 6. The density profiles of some silicate minerals including clinopyroxene, stishovite, majoritic garnet, $MgSiO_3$ perovskite, cubic and tetrahedral $CaSiO_3$ perovskites are also calculated for comparison. The data sources used were as follows: Nishihara et al. (2003) for clinopyroxene (Cpx) with $\rho_0 = 3.26$ g/cm^3; Wang et al. (1998) for majoritic garnet (Gt) with $\rho_0 = 3.71$ g/cm^3 (Ono et al. 2001); Nishihara et al. (2005) for stishovite (St) with $\rho_0 = 4.25$ g/cm^3 (Ono et al. 2002); Shim et al. (2000) for cubic Ca-perovskite (C-CaPv) with $\rho_0 = 4.23$ g/cm^3; Ono et al. (2004b) for tetragonal Ca-perovskite (T-CaPv) with $\rho_0 = 4.25$ g/cm^3; and Ono et al. (2004a) for Mg-perovskite (Mg-Pv) with $\rho_0 = 4.35$ g/cm^3 (Guignot and Andrault 2004). Generally, the chemical composition of each phase changes with increasing pressure and temperature in natural systems (Irifune et al. 1994; Ono 1998; Ono et al. 2001). However, due to the lack of available experimental data, the chemical composition of each phase was assumed to be constant to calculate the density. It should be noted the densities were calculated at room temperature since no enough thermoelastic parameters are available, though the effect of temperature on different minerals is dissimilar.

The density of monoclinic low-pressure $Ca_2AlSiO_{5.5}$ oxygen defect perovskite is larger than that of clinopyroxene, but smaller than those of other silicate minerals. The density of rhombohedral high-pressure $Ca_2AlSiO_{5.5}$ oxygen defect perovskite is larger than that of clinopyroxene and monoclinic low-pressure $Ca_2AlSiO_{5.5}$ oxygen defect perovskite and smaller than those of stishovite and Mg-perovskite. Compared with Ca-perovskite, the low-pressure and high-pressure $Ca_2AlSiO_{5.5}$ oxygen defect perovskites have low densities due to the oxygen vacancies in the structures. It is noted that in the transition zone, the density of the high-pressure $Ca_2AlSiO_{5.5}$ oxygen defect perovskite is slightly lower than that of majoritic garnet. Previous studies have shown that the mineral phases in the Earth's transition zone are dominated by ringwoodite, majoritic garnet and calcium silicate perovskite (Hirose and Fei 2002; Irifune and Tsuchiya 2007). With pressure increasing, small amount of aluminum would likely be dissolved in majorite (Bläß et al. 2004). Therefore, the low-pressure and high-pressure $Ca_2AlSiO_{5.5}$ oxygen defect perovskites are rare in the upper mantle. Although the stability of high-pressure $Ca_2AlSiO_{5.5}$ oxygen defect perovskite in the lower mantle is unknown, the dissolved aluminum in majorite may enter $CaSiO_3$ perovskite to form the oxygen defect perovskite since majorite disappears in the lower mantle. Therefore, the high-pressure $Ca_2AlSiO_{5.5}$ oxygen defect perovskite may be an potential host for Al in the Earth's lower mantle. Moreover, the low-pressure and high-pressure Ca-rich defect perovskites may exist in shock veins of meteorites with

Ca- and Al-rich composition (Kojitani et al. 2009). Additionally, a $Ca(Fe_{0.4}Si_{0.6})O_{2.8}$ oxygen-deficient perovskite was reported (Bläß et al. 2004). It suggests that $CaSiO_3$ perovskite may have the ability to accommodate a wide range of substitutions of other trivalent cations in the deep mantle.

Conclusions

1. High-pressure and room temperature in situ synchrotron X-ray diffraction experiments of low-pressure and high-pressure $Ca_2AlSiO_{5.5}$ oxygen defect perovskites have been carried out using multianvil apparatus up to 22.75 and 25.76 GPa, respectively. Fitting a third-order Birch–Murnaghan EoS to the *P–V* data yields values of $K_0 = 146.1(9)$ GPa and $K_0' = 3.64(9)$ for low-pressure phase, and $K_0 = 150.4(19)$ GPa and $K_0' = 3.16(23)$ for high-pressure phase. If K_0' was fixed at 4.0, the isothermal bulk moduli were obtained as 142.6(3) and 144.0(8) GPa for low-pressure and high-pressure phases, respectively.
2. The analysis of axial compressibilities of low-pressure high-pressure $Ca_2AlSiO_{5.5}$ oxygen defect perovskites shows that the *c*-axis is more compressible than the *a*- and *b*-axis.
3. Based on high-pressure and high-temperature data, thermoelastic property of low-pressure $Ca_2AlSiO_{5.5}$ oxygen defect perovskite was obtained as $V_0 = 827.0(3)$ Å^3, $K_T = 146.8(22)$ GPa, $K_T' = 3.55(21)$, $(\partial K_T/\partial T)_P = -0.037(2)$ GPa/K and $\alpha_T = 7.67(20) \times 10^{-5} - 3.20(30) \times 10^{-8}$ T.
4. The isothermal bulk moduli of $Ca_2AlSiO_{5.5}$ oxygen defect perovskite are about 90 GPa lower than that of $CaSiO_3$ perovskite.
5. The densities of both low-pressure and high-pressure $Ca_2AlSiO_{5.5}$ oxygen defect perovskites are larger than that of clinopyroxene, but smaller than those of majoritic garnet, stishovite, $MgSiO_3$ perovskite and $CaSiO_3$ perovskite.

Acknowledgments The $Ca_2AlSiO_{5.5}$ oxygen defect perovskite samples were kindly provided by H. Kojitani. The authors thank S. Nie for helpful discussion on the crystal structure of low-pressure $Ca_2AlSiO_{5.5}$ oxygen defect perovskite, D. Yamazaki, N. Tsujino, M. Sakurai and E. Ito for experimental helps. We thank Prof. T. Tsuchiya for his editorial handling. Critical comments and suggestion from two anonymous reviewers are helpful to improve the manuscript. The synchrotron radiation experiments were carried out at BL04B1, SPring-8, Japan (Proposal No. 2013B1257 and 2014A1736). This work was financially supported by National Natural Science Foundation of China (Grant No. 41372040), the Knowledge Innovation Program of the Institute of Geochemistry, Chinese Academy of Sciences and the Visiting Researcher's Program of the Institute for Study of the Earth's Interior, Okayama University.

References

Akber-Knutson S, Bukowinski MS, Matas J (2002) On the structure and compressibility of $CaSiO_3$ perovskite. Geophys Res Lett 29:4-1–4-4

Andrault D, Bolfan-Casanova N, Bouhifd MA, Guignot N, Kawamoto T (2007) The role of Al-defects on the equation of state of Al–(Mg, Fe)MgSiO3 perovskite. Earth Planet Sci Lett 263:167–179

Angel RJ (2001) Equations of state. Rev Miner Geochem 41:35–59

Birch F (1947) Finite elastic strain of cubic crystals. Phys Rev 71:809–924

Bläß U, Langenhorst F, Boffa-Ballaran T, Seifert F, Frost D, McCammon C (2004) A new oxygen-deficient perovskite phase $Ca(Fe_{0.4}Si_{0.6})O_{2.8}$ and phase relations along the join $CaSiO_3$–$CaFeO_{2.5}$ at transition zone conditions. Phys Chem Miner 31:52–65

Bläß U, Langenhorst F, Frost D, Seifert F (2007) Oxygen deficient perovskites in the system $CaSiO_3$–$CaAlO_{2.5}$ and implications for the Earth's interior. Phys Chem Miner 34:363–376

Brodholt JP (2000) Pressure-induced changes in the compression mechanism of aluminous perovskite in the Earth's mantle. Nature 407:620–622

Fitz Gerald J, Ringwood A (1991) High pressure rhombohedral perovskite phase $Ca_2AlSiO_{5.5}$. Phys Chem Miner 18:40–46

Guignot N, Andrault D (2004) Equations of state of Na–K–Al host phases and implications for MORB density in the lower mantle. Phys Earth Planet Inter 143:107–128

Hirose K (2002) Phase transitions in pyrolitic mantle around 670-km depth: Implications for upwelling of plumes from the lower mantle. J Geophys Res, 107. doi:10.1029/2001JB000597

Hirose K, Fei Y (2002) Subsolidus and melting phase relations of basaltic composition in the uppermost lower mantle. Geochim Cosmochim Acta 66:2099–2108

Holland TJB, Redfern SAT (1997) UNITCELL: a nonlinear least-squares program for cell-parameter refinement and implementing regression and deletion diagnostics. J Appl Crystallogr 30:84

Irifune T, Tsuchiya T (2007) Phase transitions and mineralogy of the lower mantle. In: Price D (ed) Treatise on geophysics, vol 2. Elsevier, Amsterdam, pp 33–62

Irifune T, Ringwood AE, Hibberson WO (1994) Subduction of continental crust and terrigenous and pelagic sediments: an experimental study. Earth Planet Sci Lett 126:351–368

Kanzaki M, Xue X, Wu Y (2012) Crystal structure of low-pressure $Ca_2AlSiO_{5.5}$ defect perovskite (Abstract). Japan Geoscience Union Meeting, Chiba, Japan

Kesson S, Fitz Gerald J, Shelley J, Withers R (1995) Phase relations, structure and crystal chemistry of some aluminous silicate perovskites. Earth Planet Sci Lett 134:187–201

Kojitani H, Wakabayashi Y, Tejima Y, Kato C, Haraguchi M, Akaogi M (2009) High-pressure phase relations in $Ca_2AlSiO_{5.5}$ and energetics of perovskite-related compounds with oxygen defects in the $Ca_2Si_2O_6$–$Ca_2Al_2O_5$ join. Phys Earth Planet Inter 173:349–353

Kudo Y, Hirose K, Murakami M, Asahara Y, Ozawa H, Ohishi Y, Hirao N (2012) Sound velocity measurements of $CaSiO_3$ perovskite to 133GPa and implications for lowermost mantle seismic anomalies. Earth Planet Sci Lett 349:1–7

Litasov KD, Ohtani E, Suzuki A, Funakoshi K (2007) The compressibility of Fe- and Al-bearing phase D to 30 GPa. Phys Chem Miner 34:159–167

Mao HK, Chen LC, Hemley RJ, Jephcoat AP, Wu Y, Bassett WA (1989) Stability and equation of state of $CaSiO_3$-perovskite to 134 GPa. J Geophys Res 94:17889–17894

Navrotsky A (1999) Mantle geochemistry-a lesson from ceramics. Science 284:1788–1789

Nishihara Y, Takahashi E, Matsukage K, Kikegawa T (2003) Thermal equation of state of omphacite. Am Miner 88:80–86

Nishihara Y, Nakayama K, Takahashi E, Iguch T, Funakoshi K (2005) *P–V–T* equation of state of stishovite to the lower mantle transition zone conditions. Phys Chem Miner 31:660–670

Noguchi M, Komabayashi T, Hirose K, Ohishi Y (2013) High-temperature compression experiments of $CaSiO_3$ perovskite to lowermost mantle conditions and its thermal equation of state. Phys Chem Miner 40:81–91

Ono S (1998) Stability limits of hydrous minerals in sediment and mid-ocean ridge basalt compositions: implications for water transport in subduction zones. J Geophys Res 103:18253–18267

Ono S, Ito E, Katsura T (2001) Mineralogy of subducted basaltic crust (MORB) from 25 to 37 GPa, and chemical heterogeneity of the lower mantle. Earth Planet Sci Lett 190:57–63

Ono S, Suto T, Hirose K, Kuwayama Y, Komabayashi T, Kikegawa T (2002) Equation of state of Al-bearing stishovite to 40 GPa at 300 K. Am Miner 87:1486–1489

Ono S, Kikegawa T, Iizuka T (2004a) The equation of state of orthorhombic perovskite in a peridotitic mantle composition to 80 GPa: implications for chemical composition of the lower mantle. Phys Earth Planet Inter 145:67–74

Ono S, Ohishi Y, Mibe K (2004b) Phase transition of Ca-perovskite and stability of Al-bearing Mg-perovskite in the lower mantle. Am Miner 89:1480–1485

Ricolleau A, Fei Y, Cottrell E, Watson H, Deng L, Zhang L, Fiquet G, Auzende A-L, Roskosz M, Morard G, Prakapenka V (2009) Density profile of pyrolite under the lower mantle conditions. Geophys Res Lett 36. doi:10.1029/2008GL036759

Ross N, Angel R, Seifert F (2002) Compressibility of brownmillerite ($Ca_2Fe_2O_5$): effect of vacancies on the elastic properties of perovskites. Phys Earth Planet Inter 129:145–151

Saxena S, Zhang J (1990) Thermochemical and pressure–volume–temperature systematics of data on solid, exzamples: tungsten and MgO. Phys Chem Miner 17:45–51

Shim S, Duffy T, Shen G (2000) The stability and P–V–T equation of state of CaSiO3 perovskite in the Earth's lower mantle. J Geophys Res 105:25955–25968

Shim S, Jeanloz R, Duffy T (2002) Tetragonal structure of $CaSiO_3$ perovskite above 20 GPa. Geophys Res Lett 29:2166

Stixrude L, Lithgow-Bertelloni C, Kiefer B, Fumagalli P (2007) Phase stability and shear softening in $CaSiO_3$ perovskite at high pressure. Phys Rev B 75:24108

Tsuchiya T (2003) First-principles prediction of the *P–V–T* equation of state of gold and the 660-km discontinuity in Earth's mantle. J Geophys Res 108:2462

Wang Y, Weidner D, Guyot F (1996) Thermal equation of state of $CaSiO_3$ perovskite. J Geophys Res 101:661–672

Wang Y, Weidner D, Zhang J, Gwanrnesia GD, Liebermann R (1998) Thermal equation of state of garnets along the pyrope-majorite join. Phys Earth Planet Inter 105:59–71

Zhai S, Xue W, Yamazaki D, Shan S, Ito E, Tomioka N, Shinojuku A, Funakoshi K (2011) Compressibility of strontium orthophosphate $Sr_3(PO_4)_2$ at high pressure. Phys Chem Miner 38:357–361

Zhai S, Yamazaki D, Xue W, Ye L, Xu C, Shan S, Ito E, Yoneda A, Yoshino T, Guo X, Shimojuku A, Tsujino N, Funakoshi K (2013) *P–V–T* relations of γ-$Ca_3(PO_4)_2$ tuite determined by in situ X-ray diffraction in a large-volume high-pressure apparatus. Am Miner 98:1811–1816

Zhang J, Weidner D (1999) Thermal equation of state of aluminum-enriched silicate perovskite. Science 284:782–784